A "Numerical Mesoscope" for the Investigation of Local Fields in Rate-Dependent Elastoplastic Materials at Finite Strain

Halim Haddadi, Cristian Teodosiu, S. Héraud, L. Allais, André Zaoui

A "Numerical Mesoscope" for the Investigation of Local Fields in Rate-Dependent Elastoplastic Materials at Finite Strain

H. Haddadi, C. Teodosiu
LPMTM-CNRS, Université Paris-Nord, Institut Galilée
Avenue J.-B. Clément, 93430 Villetaneuse Cedex, France
halim.haddadi@lpmtm.univ-paris13.fr, teodosiu@galilee.univ-paris13.fr

S. Héraud
Harting E.U.R.L.
181 avenue des Nations, Z.A.C. Paris-Nord II, 95972 Roissy CDG Cedex, France

L. Allais
Commissariat à l'Energie Atomique, CEREM/SRMA
Saclay, 91191 Gif-sur-Yvette Cedex, France

A. Zaoui
Laboratoire de Mécanique des Solides, CNRS-Ecole Polytechnique
91128 Palaiseau Cedex, France
zaoui@lms.polytechnique.fr

Abstract: We propose a "numerical mesoscope" which could be used for the analysis of the local mechanical fields over small critical areas of microheterogeneous materials, in order to predict the local initiation of specific deformation or damage mechanisms. The subdomain under investigation is embedded in a very large homogeneous matrix obeying the overall behavior of the studied material, as determined experimentally. This matrix is subjected to homogeneous stress or strain boundary conditions and the homogeneous elements of the subdomain and their interfaces are given their known or assumed constitutive behavior. A finite element analysis is then performed on the whole body by making use of different constitutive equations within the subdomain and in the surrounding matrix. The general methodology of this approach is reported and applied to a metallic rate-dependent elastoplastic polycrystal and to microheterogeneous subdomains consisting of given multicrystalline patterns whose grains obey crystalline elastoplastic constitutive equations of Schmid type at finite strain. Application to the intergranular creep damage of a stainless steel shows a good agreement between the largest computed normal stresses on the grain boundaries and the observed debonded boundaries of the actual material.

Keywords: Numerical simulation, polycrystals, rate-dependent elastoplasticity, finite strain, creep-damage.

1. Principle of the "numerical mesoscope"

The knowledge of the local mechanical fields over small critical areas of microheterogeneous materials is generally needed for a better understanding and prediction of the initiation of specific deformation or damage mechanisms, such as twinning, phase transformation, grain boundary debonding, etc. Such regions can be in fact much smaller than the representative volume element (RVE), so that, unlike the RVE, they cannot be considered as subjected to homogeneous strain or stress boundary conditions. For example, the intergranular failure of metallic polycrystals depends on the mechanical state over a few adjacent grains, whereas the RVE can extend over millions of grains and the average strain or stress state in the RVE is of no help for predicting grain boundary debonding. On the other hand, direct numerical simulation of aggregates of several thousands of grains, i.e., large enough to be a good approximation of a RVE, in addition to being hardly tractable, cannot yield reliable predictions of debonding in actual polycrystals: although they are statistically representative of these polycrystals with respect to their crystallographic texture or their average grain shape, they cannot coincide with them at the scale of a few grains.

In what follows, by applying the concept of "numerical mesoscope" (Héraud et al. [6]), we consider the microheterogeneous subdomain under investigation as embedded with a perfect interface in a large homogeneous matrix. This matrix, which obeys the experimentally defined overall behavior of the studied material, is subjected to homogeneous stress or strain boundary conditions, so that, due to its own mechanical response, different mechanical conditions, which are expected to be more realistic, are transferred to the boundary of the considered subdomain. Adequate (known or assumed) local constitutive equations are defined at each point of the heterogeneous subdomain: their nature can be different from that of the matrix (e.g., for a polycrystal, they can be of a phenomenological type for the matrix and of crystalline Schmid type for the grains of the subdomain). Nevertheless, a single finite element analysis has to be performed on the whole body through some "numerical mesoscope", so as to yield the local mechanical state within the heterogeneous subdomain. Since this subdomain is not a RVE, the resulting analysis does not reduce to the classical *concentration* or *localization* procedure of usual homogenization schemes; in some sense, it could be seen as a *back-localization* analysis, which focuses on some specific critical areas within the RVE.

Since the same material is considered at the micro- and the macroscale, the local and the global constitutive equations used in the numerical analysis in the *inclusion* and in the *matrix*, respectively, have to be consistent with each other. In the following, this consistency condition is ensured through an auxiliary numerical computation: a large enough microheterogeneous RVE is generated and its overall response to a macroscopic loading is derived from the consti-

tutive equations of the constituents. The consistency condition requires this response to coincide with the macroscopic response of the actual material. Alternative solutions, which would not need such auxiliary computations, could have recourse either to a micromechanical model predicting the overall behavior from the local one or to direct measurements of the displacement field at the boundary of the considered subdomain.

This approach is now focused on the case of rate-dependent elastoplastic polycrystals (Sect. 2) and then illustrated by an application (Sect. 3) to creep-damaged grain boundaries of a stainless steel, which has been experimentally studied in parallel by use of scanning electron microscopy (SEM) for the grain shapes and of electron back-scattering diffraction (EBSD) for the lattice orientations. Additional computations are reported in Sect. 4, in order to appreciate the pertinence of the proposed approach, and possible extensions are briefly discussed in conclusion.

2. "Numerical mesoscopy" and polycrystals

2.1. CONSTITUTIVE EQUATIONS

In view of the increasing diversity of potential applications to polycrystalline materials, rate-dependent elastoplasticity has been considered. In order to simplify the search for a satisfying consistency between the local and the overall constitutive equations, we have adopted similar forms for these equations at both scales. The resulting constitutive equations are derived from those proposed by Anand and associates (Anand [1], Brown et al. [3]) for the flow rule and by Kocks [7] for the description of the intragranular work-hardening. A finite strain formalism is needed, since, even for small macroscopic deformations, strains can be large at the local level. At the macroscopic scale, an isotropic formulation is adopted, for sake of simplicity. The strain-hardening of the material is described by a scalar internal state variable, called S. The plastic strain rate and the evolution equation of S are given by

$$\dot{\bar{E}}^{\mathrm{p}} = A \left[\sinh\left(\frac{\bar{\Sigma}}{S}\right)\right]^{\frac{1}{m}} \exp\left(-\frac{Q}{RT}\right), \tag{1}$$

$$\dot{S} = H_0 \left|\frac{S_{\mathrm{sat}} - S}{S_{\mathrm{sat}} - S_0}\right|^a \operatorname{sgn}(S_{\mathrm{sat}} - S_0)\, \dot{\bar{E}}^{\mathrm{p}}, \tag{2}$$

where $\dot{\bar{E}}^{\mathrm{p}}$ and $\bar{\Sigma}$ are the macroscopic von Mises equivalent strain rate and stress respectively, Q an apparent activation energy, T the absolute temperature, R the perfect gases constant; S_0 is the initial value of S and $S_{\mathrm{sat}} = \bar{S}(Z/A)^n$ its limit value, where $Z = \dot{\bar{E}}^{\mathrm{p}} \exp(Q/RT)$ denotes the Zener-Holomon parameter. Thus, apart from the elastic moduli, the material parameters are $A, m, Q/R, H_0, a, S_0, \bar{S}$ and n.

Similar equations are adopted at the crystal level for the relation between the plastic shear rate $\dot{\gamma}^{(s)}$ and the resolved shear stress $\tau^{(s)}$ on the slip system (s), namely

$$\dot{\gamma}^{(s)} = \alpha \left[\sinh\left(\frac{\tau^{(s)}}{\tau_c^{(s)}}\right)\right]^{\frac{1}{m}} \exp\left(-\frac{Q}{RT}\right) \operatorname{sgn}(\tau^{(s)}), \tag{3}$$

$$\dot{\tau}_c^{(s)} = \sum_u a^{(su)}\, h(z^{(u)}, \tau_c^{(u)})\, |\dot{\gamma}^{(u)}|, \tag{4}$$

with

$$h(z^{(u)}, \tau_c^{(u)}) = h_0(z^{(u)}) \left|\frac{\tau_{sat}^u(z^{(u)}) - \tau_c^{(u)}}{\tau_{sat}^u(z^{(u)}) - \tau_0^{(u)}}\right|^a \operatorname{sgn}(\tau_{sat}^{(u)}(z^{(u)}) - \tau_0^{(u)}), \tag{5}$$

$$\tau_{sat}^{(u)}(z^{(u)}) = \bar{\tau}\left(\frac{z^{(u)}}{\alpha}\right)^n, \qquad z^{(u)} = \dot{\gamma}^{(u)} \exp\left(\frac{Q}{RT}\right). \tag{6}$$

For sake of consistency with the macroscopic equations, material parameters $m, Q/R, a$ and n are the same at both levels. The hardening matrix $a^{(su)}$ may be used in the usual simple form $q + (1-q)\delta^{(su)}$, with $q \geq 1$, in order to take latent hardening into account. Further simplifications, which are considered in the sequel, consist of setting $h_0(z^{(u)}) = h_0$ and $\tau_0^{(u)} = \tau_0$, where h_0 and τ_0 are constants, i.e. independent of the slip system (u). The additional material parameters at the microscale then reduce to α, q, h_0, τ_0 and $\bar{\tau}$.

2.2. NUMERICAL INTEGRATION

The finite element numerical treatment has been carried out by using an extension for the crystalline pattern elaborated by Héraud [5] of the 3D-code EPVIM3D developed by Haddadi [4]. At the local scale, a forward gradient scheme is used for the shear increments $\Delta\gamma^{(s)}$, while the shear stress increments $\Delta\tau^{(s)}$ and $\Delta\tau_c^{(s)}$ are linearized. The basic equation reads

$$\Delta\gamma^{(s)} = [(1-\beta)\,\dot{\gamma}^{(s)}(t) \,+\, \beta\,\dot{\gamma}^{(s)}(t+\Delta t)]\,\Delta t,$$

where β has a fixed value (around $2/3$). A first-order Taylor development is used for the derivation of $\dot{\gamma}^{(s)}(t+\Delta t)$. A similar treatment is used at the macroscopic scale. Each finite element has 8 nodes and 8 integration points, with use of reduced integration for the volumetric part of the deformation and of isoparametric shape functions. The time increments are optimized so as to be shorter whenever the intracrystalline shear rates are larger. Specific routines have been developed in order to derive the stress vectors on the grain boundaries from the stress tensors evaluated within the adjacent grains.

3. Application to a creep-damaged stainless steel

The foregoing concept of "numerical mesoscopy" has first been applied to the interpretation of grain-boundary debonding in a specimen of AISI316 stainless steel. This specimen was subjected to a creep test up to fracture, under370 MPa at $550\,^{\circ}$C during 395 hours and then cut along a longitudinal cross-section. A small area of about 50 grains and 100 μm diameter, exhibiting several debonded grain boundaries, has been selected in this section. The geometry, as well as the lattice orientations of 35 grains of the central multicrystal, have been determined through SEM observation and EBSD analysis. The problem was then to simulate this crystalline area as central pattern of our mesoscope, embedded in a large homogeneous matrix, subjected to the macroscopic loading of the actual creep test, and to compute the normal stresses on the grain boundaries of the pattern in order to look for any correlation between largest computed normal stresses and the most damaged boundaries.

Overall creep behavior. The constitutive equations of the studied material was first to be determined. This has been done by Héraud [5], using the experimental creep data obtained for this material at three different temperatures ($550, 600$ and $650\,^{\circ}$C) and, for each temperature, under three different load levels (from 150 MPa to 420 MPa according to the temperature). A preliminary rough analysis has first been performed in order to enter initial parameters in the optimization code SIDOLO [8]. After a small number of iterations, we have got the following parameters (in addition to the Young modulus,$E = 143$ GPa, and the Poisson ratio, $\nu = 0.33$): $A = 1.96 \times 10^7$ s^{-1}, $m = 0.053$, $Q/R = 34200$ K, $H_0 = 3470$ MPa, $a = 0.8$, $S_0 = 36$ MPa, $\bar{S} = 102$ MPa and $n = 0.16$. The global constitutive equations (1) and (2) are thus determined.

Local constitutive equations. They have been identified from the fitting of the creep response of a simulated polycrystal whose grains obey equations (3) to (6) to the experimental data. This model polycrystal has first been defined for an isotropic copper polycrystal already studied by Anand et al. [2]. The result was a FEM model consisting of a cubic aggregate of 1000 cubic grains of the same size, where each grain is represented by one finite element. Application to our studied material and experimental data, through the same identification procedure as before, has led to the following local parameters: $\alpha = 0.5 \times 10^7$ s^{-1}, $h_0 = 920$ MPa, $\tau_0 = 37$ MPa, $\bar{\tau} = 120$ MPa and $q = 1.4$, to be used for the considered creep test at $T = 550\,^{\circ}$C under 370 MPa.

FEM computation. As a first approximation, a single three-dimensional layer of elements has been considered. The matrix area is about five times larger than the crystalline pattern. The grain boundaries are normal to the layer. The whole body has been meshed by use of the SIMAIL software from Simulog

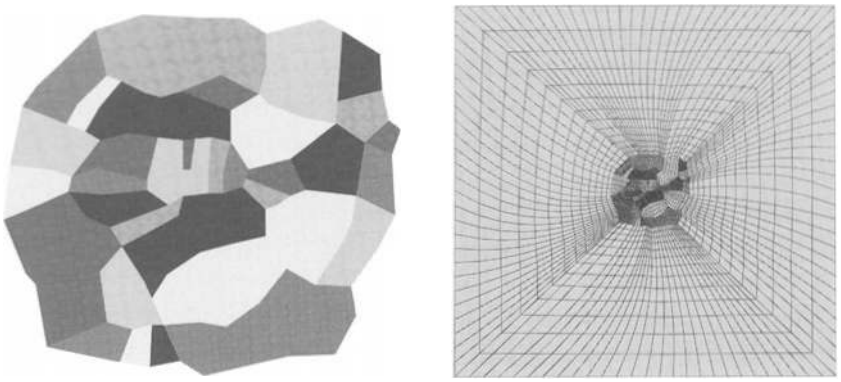

Figure 1. The 35-grain multicrystalline aggregate and the mesh of the whole mesoscopic domain.

(1145 elements for the multicrystal and 1430 for the matrix; see Figure 1). The four lateral faces, which are parallel to the creep direction, are supposed free, while the remaining two faces, which are perpendicular to the creep direction, are subjected to an imposed traction. In addition, any rigid-body displacement has been suppressed by adequate displacement boundary-conditions. For such boundary conditions, 15,786 degrees of freedom are needed (Héraud [5]).

Results. The simulation of the creep test has been performed up to277 hours, whereas fracture occurred after 395 hours in the actual test. The considered multicrystal proved to be stiffer than the matrix on average: he was less deformed and more stressed, which agrees with the fact that the selected pattern looked especially damaged. Among several local analyses of the stress and strain fields in the grains (Héraud [5]), special attention has been paid to the distribution of the stress vectors on the grain boundaries. Whereas no correlation was detected between the shear stress level and the damage amplitude on these boundaries, a definite one existed between the largest computed normal stresses and the experimentally debonded boundaries (compare e.g. the grain boundaries denoted by GB1, GB2 and GB3 in Figures 2 and 3). Although this conclusion can be appreciated as an encouraging evidence for the pertinence of the concept of "numerical mesoscope", further investigations have been performed in order to corroborate this statement.

4. Pertinence of the numerical mesoscope

As argued in the introduction, the main reason for developing such a complex simulation tool lies in the fact that any local mechanical analysis on subdomains which are smaller than the RVE cannot be sensibly performed through direct application of the macroscopic boundary conditions to the boundary of these

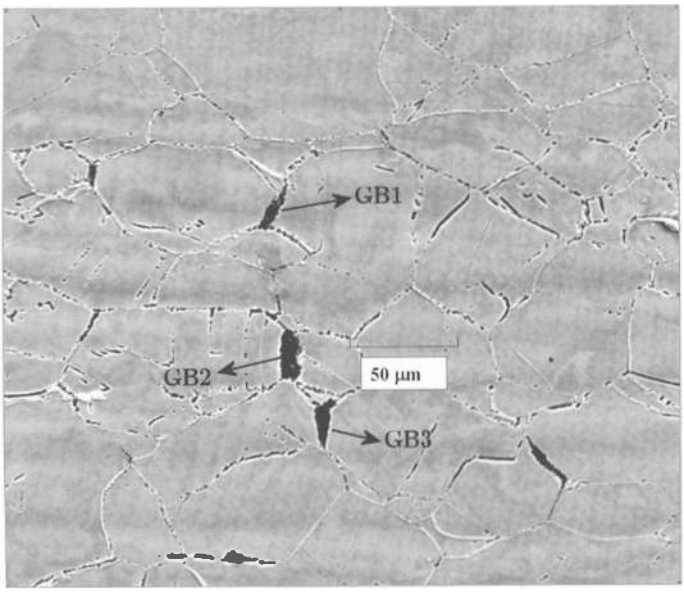

Figure 2. Location of debonded grain boundaries in the actual material.

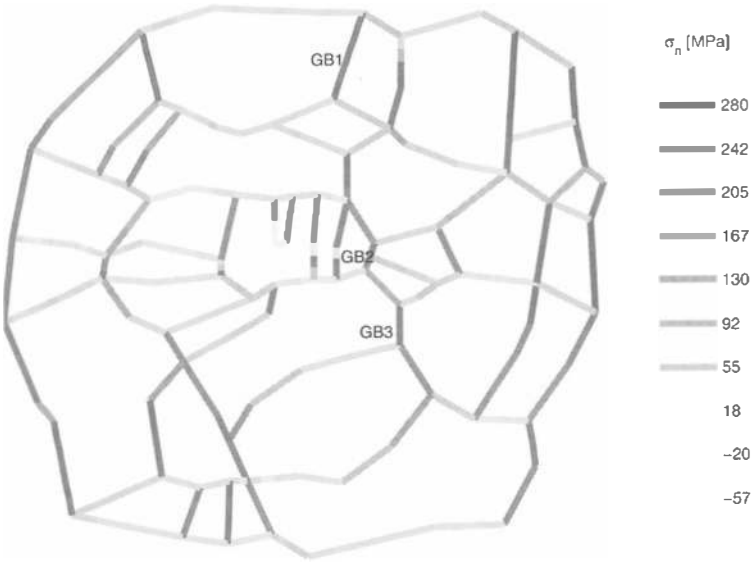

Figure 3. Distribution of the normal component of the stress vector on the grain boundaries of the simulated multicrystal.

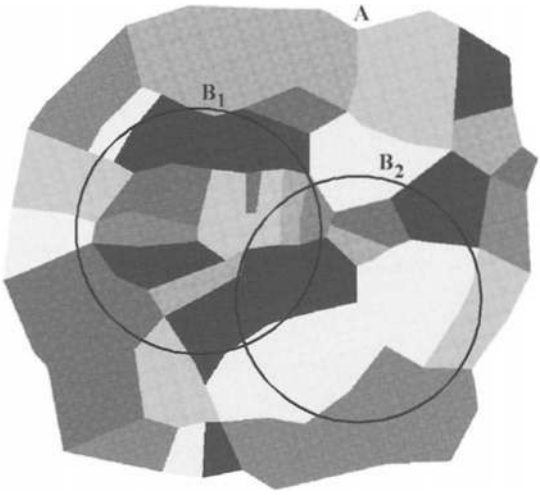

Figure 4. The initial 35-grain multicrystal (sample A) and the extracted samples B_1 and B_2.

subdomains. When experimental data of the actual displacement or traction fields on this boundary are not available, it is proposed to embed the subdomain of interest in a quasi-infinite matrix obeying the experimentally defined overall behavior and subjected to the macroscopic boundary conditions, so as to load the investigated subdomain in a more realistic way. Conversely, the pertinence of the numerical mesoscope can be appreciated *a posteriori* by comparing the actual displacement or traction fields on the boundary of the simulated subdomain, as they result from the whole FEM computation, with those which would be associated to the average macroscopic strain or stress tensors.

Such an analysis has been performed on the above reported application and it resulted in strong differences between these fields (Héraud [5]), which could have been considered as a sufficient justification of the rather lengthy numerical procedure required by the numerical mesoscope. However, this reasoning has been considered not enough conclusive, because the angular geometry of the multicrystal boundary, which results in strong local stress concentrations, may indeed affect the comparison with the rather smooth macroscopic boundary conditions.

That is the reason why further numerical analyses have been performed on subdomains cut out from the initial 35-grain multicrystal, which will be called sample A from now on. Two circular disks, say samples B_1 and B_2, have been extracted from sample A, both of them of the same size, but located at two different places in the multicrystal and consisting of a smaller number of grains, namely 15 and 12 grains, respectively (see Figure 4). In order to shorten the computation times for the same simulated creep test, some material parameters

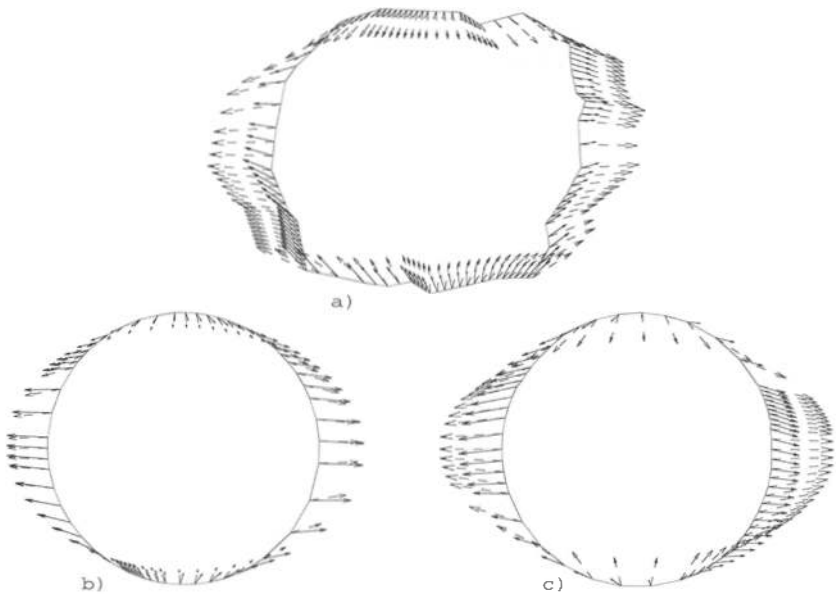

Figure 5. In-plane components of the relative displacements on the boundary of each of the three disk-shaped samples with respect to the centre of its top surface (solid vectors), compared with those derived from the respective average displacement gradients (dashed vectors). a) Sample A, b) sample B_1, and c) sample B_2.

where modified in a similar way for both the matrix and the constituent crystals, so as to lower the global and local creep compliances. After a given creep time, the volume average of the displacement gradient tensor, say $\boldsymbol{H}$, was calculated over each multicrystalline sample, as well as the relative displacements $\boldsymbol{u}$ of the boundary of each disk-shaped sample with respect to the centre of its top surface. Figure 5 shows the in-plane components of these relative displacements on the boundary of each of the three samples (solid vectors) compared with those derived from the average displacement gradient $\boldsymbol{H}$ (dashed vectores).

It is clearly seen from these results that the actual boundary conditions on the samples differ significantly from the macroscopic ones. Indeed, since the latter result from a homogeneous displacement gradient, the tips of the corresponding displacement vectors on the circular boundaries of samples B_1 and B_2 are smoothly distributed on ellipses, whereas the displacement fields resulted from the simulations on their boundaries vary more sharply from point to point. It is worth noting that these differences are more visible on sample B_2, which has been subjected to a larger plastic deformation, than on sample B_1, which

was closer to an elastic state. Notwithstanding, even sample B_1 displays a significant change in the *direction* of the calculated displacement vectors with respect to the homogeneous boundary conditions, especially on the bottom of its circular boundary. It may be concluded that the ensemble of these results do substantiate the pertinence of the numerical mesoscope.

5. Conclusion

Further developments are obviously needed from this kind of "prototype". In addition to computational improvements (parallel computations, improved automatic meshing, etc.), two kinds of mechanical developments are currently in progress. On the one hand, a larger number of plane layers are to be considered, consisting either of crystal or of matrix material, with oblique grain boundaries. On the other hand, imperfect interfaces are developed within the crystalline pattern, in view of modeling debonding or sliding grain boundaries. It is expected that this will result in extended interpretation schemes, especially in the field of the identification of crystal constitutive equations from micromechanical measurements over grains, as well as in the complex field of the micromechanics of damage.

References

[1] Anand, L. (1985). Constitutive equations for hot-working of metals. *Int. J. Plasticity*, **1**, 213–231.

[2] Anand, L., Balasubramanian, S. and Kothari, K. (1996). Constitutive modeling of polycrystalline metals at large strains. In: *Large Plastic Deformation of Crystalline Aggregates*, C. Teodosiu (ed.), CISM Courses and Lectures No. 376, Springer Verlag, Wien, New York, 109–172.

[3] Brown, S.B., Kim, K.H. and Anand, L. (1989). An internal variable constitutive model for the hot working of metals. *Int. J. Plasticity*, **5**, 95–130.

[4] Haddadi, H. (1996). *Matériaux composites à matrice métallique: modélisation du comportement thermo-élastoviscoplastique et résolution de problèmes aux limites 3D*. PhD Thesis, Université Paris 13, France.

[5] Héraud, S. (1998). *Du polycristal au multicristal: élaboration d'un mésoscope numérique pour une analyse locale en élastoviscoplasticité*. PhD Thesis, Ecole polytechnique, Palaiseau, France.

[6] Héraud S., Allais L., Haddadi H., Marini B., Teodosiu C. and Zaoui A. (1998). Du polycristal au multicristal: vers un mésoscope numérique. *J. Phys. IV France*, 8:4-27-32.

[7] Kocks, U.F. (1987). Constitutive behaviour based on crystal plasticity. In: *Constitutive Equations for Creep and Plasticity*, A.K. Miller (ed.), Elsevier Appl. Sci., London, 1–88.

[8] SIDOLO, Notice d'utilisation (1993). Ecole des Mines de Paris, France.